ARTICLE

Designed Polynuclear Lanthanide Complexes for Quantum Information Processing

Received 00th January 20xx,
Accepted 00th January 20xx

DOI: 10.1039/x0xx00000x

David Aguilà,*[a,b] Olivier Roubeau [c,d] and Guillem Aromí *[a,b]

The design of dissymmetric organic ligands featuring combinations of 1,3-diketone and 2,6-diacetylpyridine coordination pockets has been exploited to produce dinuclear and trinuclear lanthanide-based coordination compounds. These molecules exhibit two or more non-equivalent Ln ions, most remarkably enabling the access to well-defined heterolanthanide compositions. The site-selective disposition of each metal ion within the molecular entities allows to study each centre individually as a spin-based quantum bit, affording unparalleled versatility for quantum gate design. The inherent weak interaction between the Ln ions permits the performance of multi-qubit quantum logical operations realized through their derived magnetic states, or implementing quantum-error correction protocols. The different studies performed to date on these systems are revised, showing their vast potential within spin-based quantum information processing.

Introduction

Lanthanide compounds have been widely exploited due to their exceptional physical properties,[1-10] specially in their most common oxidation state (+3), when they exhibit the electronic configuration [Xe]4f n (n = 0 to 14). The coupling between the spin and orbital magnetic moments of the 4f electrons, particularly protected from external perturbations by full 5s and 5p electronic shells, generates a ladder of states that furnishes a rich variety of 4*f*–4*f* transitions spanning the near infrared (NIR) to the UV and visible region.[11-13] These transitions are formally forbidden, but the excites states can be accessed by energy transfer processes that lead to the emission phenomenon called sensitized metal luminescence.[14, 15] Such peculiarities have inspired researchers to study these materials in a wide range of applications, as in agents for optical and magnetic resonance imaging[14, 16] or devices for light-emitting diodes.[17, 18] In addition, the shielding of these electrons makes the states of these ladders to be only perturbed by the crystal fields, which split its states into the so-called Stark levels by energies ranging from the microwave region to 100 cm^{-1} at the most. These levels respond differently to an external magnetic field, thus generating an energy barrier to the inversion of the magnetization of each individual ion.[19, 20] These properties have allowed to consider lanthanide complexes for single-molecule magnetic information storage.[20-24] In the last years, lanthanide molecules have also been exploited for spin-based quantum information processing (QIP), considering the two low-lying magnetic states of Ln(III) ions as the realization of a quantum bit (the basic information unit of the quantum computer).[25, 26] In contrast to their classical counterpart, the quantum bit (or qubit) is defined not only in its two quantum states (i.e., spin up and spin down, or $|0\rangle$ and $|1\rangle$) but also in any arbitrary quantum superposition of them ($|\psi\rangle = \alpha|0\rangle + \beta|1\rangle$). This and other resources inherent to quantum mechanics allows QIP to perform tasks unachievable by current computation technologies. Thus, several quantum systems are being investigated to provide the hardware for this new type of computers. Among them, we can find the quantized levels of superconducting circuits,[27-29] the electronic states of trapped atoms or ions,[30, 31] or the use of polarization states of photons.[32, 33]

Exploiting molecules to embed spin-based qubits offers important advantages compared to other technologies, since they can be produced in large scale and can be easily tuned by chemical methods.[34] One type of molecules studied extensively as spin-based qubits are the series of clusters with formula $(R_4N)[Cr_7NiF_8(O_2CR')_{16}]$, which consist of a ring with the eight metals bridged pairwise by one F^- and two carboxylate ligands. The antiferromagnetic coupling between adjacent metals leads to an S = ½ spin ground state, which encodes the qubit.[35] The quantum coherence[36] and ability of these rings to associate into complex supramolecular structures have been studied intensely.[37, 38] In contrast to clusters, monometallic complexes do not present the need to isolate an S = ½ spin ground state from excited states. Of the possible metals, Cu(II) and V(IV) have been the most investigated[39, 40] and their quantum coherence optimized progressively.[41-44] In this context, Ln-based compounds have shown particular appealing characteristics. First, they typically exhibit large separations between the $\pm m_J$ ground state and the first excited state, allowing to use the former as an effective S = ½ two-level system and thus embody

[a] Departament de Química Inorgànica i Orgànica, Secció Química Inorgànica, Universitat de Barcelona, Barcelona, Spain.
[b] Institute of Nanoscience and Nanotechnology of the University of Barcelona (IN2UB), Barcelona, Spain.
[c] Instituto de Nanociencia y Materiales de Aragón (INMA), CSIC-Universidad de Zaragoza, Zaragoza, Spain.
[d] Departamento de Física de la Material Condensada, Universidad de Zaragoza, Zaragoza, Spain

the qubit states. Since the *g* factor of these doublets is usually very large, the qubit computational basis is highly polarizable, therefore offering better initialization capacities. In addition, the specific case of Gd(III) allows the possibility to encode several qubits in the magnetic states of one single Ln ion, exempt of spin orbit coupling (SOC), exploiting the high spin ground state and multiple transitions between different m_J states.[45] Finally, most Ln ions have isotopes with nuclear spin, which allows using the derived electronuclear transitions to define multiple qubits or n-qudits (a quantum system with n-quantum levels that can be coherently manipulated).[46]

Quantum transitions within a spin-based qubit can be driven coherently using electromagnetic pulses. The resulting magnetic states must conserve their quantum coherence for a given time, called phase-memory time, T_M, during which the information can be manipulated. This capacity was shown, for example, in a Gd^{III}-doped polyoxometalate material ($[Gd_xY_{1-x}(P_5W_{30}O_{120})]^{12-}$). For this compound, a coherence time of 410 ns was estimated for the superposition of a targeted pair of quantum states.[47] Similarly, coherent manipulations were observed within the ground-state doublet of a mononuclear compound doped with Yb^{III} ($[Yb_xLu_{1-x}(trensal)]$). Here all the possible electron-spin rotations with conservation of the nuclear spin were detected at specific magnetic fields and their quantum coherence characterized using, respectively, continuous wave and pulsed X-band EPR measurements on single-crystals.[48] Those studies, based on magnetically diluted compounds, evidenced the effect of magnetic dipolar interactions as the main source of decoherence. However, isolating the spin qubit in a diamagnetic matrix precludes interaction between them, and thus its role in multi-qubit logical operations. Decoherence problems caused by magnetic field fluctuations can be diminished when operating with atomic clock transitions, particularly protected from local field variations. This approach was shown in a Ho^{III}-molecular nanomagnet, where the holmium ion is encapsulated by two molecular tungsten oxide moieties ($[Ho(W_5O_{18})_2]^{9-}$).[49] This strategy allowed observing coherence times up to 8.4 microseconds, even for a highly concentrated sample.

The realization of algorithms for quantum computing requires a universal set of quantum gates (qugates). The latter are fundamental quantum logic operations brought about by one or several qubits. The quantum versions of the CNOT and SWAP operations constitute archetypes of two-qubit qugates. In fact, the former, together with individual qubits are a universal set. The computational basis of two-qubit gates span the four possible combinations of two qubits, $|11\rangle$, $|10\rangle$, $|01\rangle$ and $|00\rangle$. The CNOT flips the state of the second (target) qubit only when the first (control) qubit resides in a particular state, for example in the state $|1\rangle$ or spin up (ie. $|11\rangle \leftrightarrow |10\rangle$). On the other hand, the SWAP gate exchanges the state of both qubits when those are in a different state (ie. $|01\rangle \leftrightarrow |10\rangle$). Chemistry offers the possibility to incorporate two qubits within one molecule and confer them the ability to realize qugates. These two qubits need to be addressable, thus exhibit a different response to the external stimulus used to manipulate them. In the case of spin-based qubits the ideal technology for manipulating them is EPR, thus, addressable qubits must have different *g* factors. In addition, conditional operations require an interaction between qubits. However, the interaction must be weak enough so that both, factorized and entangled states are possible. All these requirements can be satisfied through chemical design, for example through incorporation of two lanthanides within molecules in the appropriate conditions.[34] Molecules hosting several lanthanides could actually allow the realization of multi-qubit quantum gates of two or even more qubits.[25, 26] or could be used to simplify the implementation of other complicated operations, such as quantum error corrections (see below), which otherwise require artificially wiring up several qubits. Another approach to address these challenges proposes to use the eight spin-orbit free, internal spin levels of the Gd ion within molecules. These spin states in the compound $[Gd(H_2O)(P_5W_{30}O_{110}]^{12-}$, for example, were exploited to perform operations using three qubits.[45] Moreover, all transitions were found to be coherently controlled, with times ranging from 470 to 600 ns at 6 K.

Some years ago, we decided to explore the synthesis of polynuclear lanthanide complexes as possible multi-qubit qugates, based on the design of organic ligands able to encapsulate more than one Ln ion in different environments. Originally, the design of the asymmetric ligand H_3LA (Scheme 1) allowed the production of a complete series of dinuclear homometallic [LnLn] species featuring non-equivalent metal ions, thus potentially able to perform two-qubit quantum gates.[50-52] Such molecular system was further exploited to embed two different Ln ions, thus producing heterometallic [LnLn'] compounds through one-pot reactions (Figure 1), overcoming a significant synthetic challenge.[53]

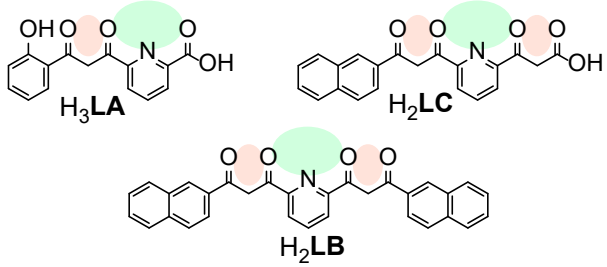

Scheme 1. Representation of ligands, previously prepared and reported by our group, H_3LA,[50] H_2LB[54] and H_2LC[55] in their fully diketone forms, emphasizing the different size of the diketone (O,O) and dipicolinate-like (O,N,O) chelating pockets, with salmon and light green colours, respectively.

Several [LnLn'] analogues were synthesized and studied (see below), underscoring the importance of incorporating different 4f ions to perform quantum logical operations. The new method discovered to isolate site-selective lanthanide heterometallic molecules was worth exploring further. Therefore, the new ligand H_2LB, able to encapsulate three different Ln ions, was produced, evidencing the potential of expanding the approach to obtain highly pure heterometallic Ln compounds with higher nuclearity. Moreover, these trinuclear entities constitute an ideal platform to perform logical operations with a quantum error correction mechanism incorporated, thus becoming a step forward towards the realization of scalable quantum computing architectures. In this perspective article, the rational design for

each type of polynuclear Ln compound is reviewed and their properties described. The potential of each system to operate on two (for [LnLn] and LnLn') or three ([LnLn'Ln]) lanthanide qubits is described, as derived from advanced spectroscopic studies and numerical simulations. In addition, the future perspectives of those Ln-based molecular processors are discussed, considering new potential designs and their role in hybrid devices.

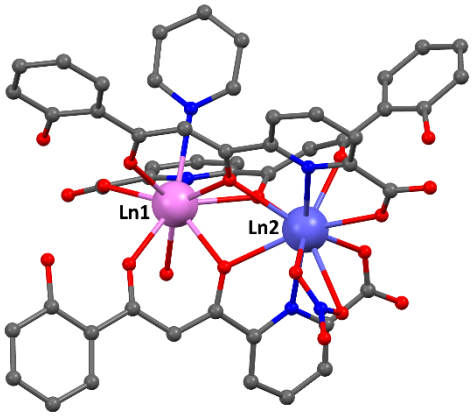

Figure 1. Representation of the characteristic molecular structure of the [LnLn] series, taken from the crystallographic data of $(Hpy)[LnLn'(HLA)_3(NO_3)(H_2O)py]$ (Ln1 = Ce, Ln2 = Er). The pyridinium cation, as well as the H atoms have been omitted for clarity. C, N and O atoms are shown in grey, blue and red, respectively.

Non-symmetric dinuclear Ln compounds as information processing devices

Dinuclear complexes featuring 4f ions are very common in the literature (more than 8000 hits in the CSD, version 5.42). However, in order to perform 2qubit logical operations, their corresponding Ln^{III} ions must be individually addressable, and thus exhibit a different magnetic response. In addition, the quantum entanglement between both qubits required to perform such operations demands that they are weakly interacting. Molecules fulfilling these criteria are scarce, since Nature favours the formation of symmetric species. In order to promote the coupling of two different Ln^{III} qubits within a molecule, we designed an asymmetric ligand, H_3LA, featuring two different chelating units, i. e., a diketone (O,O) unit and a dipicolinate-like (O,N,O) moiety (Scheme 1).[50] Satisfactorily, one-step reactions of H_3LA in pyridine with any LnX_3 salt (X = Cl^- or NO_3^-) produced the desired non-symmetric dinuclear complexes with general formula $(Hpy)[Ln_2(HLA)_3X(py)H_2O]$ (Figure 1).[50, 52] These compounds exhibit two Ln^{III} ions gathered by three partially deprotonated HLA^{2-} ligands in two different orientations. The derived molecular architecture thus imposes two different coordination sites (Ln1 and Ln2), composed of different chelating units of HLA^{2-} (Figure 2, inset). Ln1 is encapsulated by one dipicolinate-like (O,N,O) unit and two diketonate (O,O) groups, and its coordination polyhedron is completed with two terminal ligands (H_2O and pyridine). In contrast, Ln2 is coordinated to one diketonate pocket and two dipicolinate units, as well as to an X^- anion ligand (chloride or nitrate). Interestingly, the versatility of this molecular scaffold allows encapsulating any pair of 4f ions independently of their varying sizes producing, in the case of X = NO_3^-, a complete isostructural series from [LaLa] to [LuLu].[52]

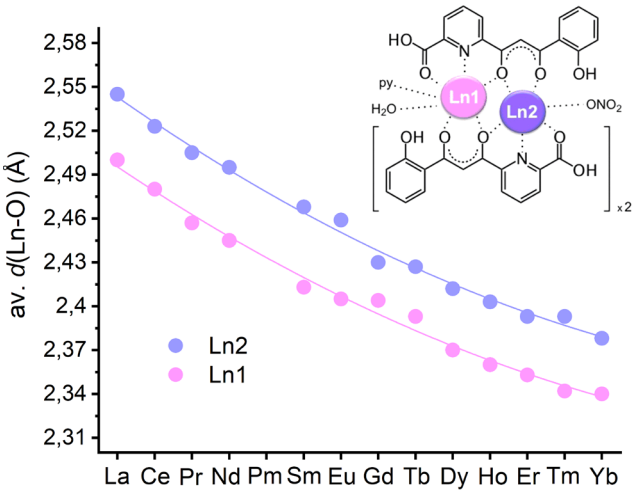

Figure 2. Plot of the average of Ln-O bond distances for all homometallic [LnLn] compounds (X = NO_3^-) considering only O atoms from HLA^{2-} ligands. The solid lines are best fits to the quadratic function $y = a + bx + cx^2$. Inset: Schematic representation of the anionic complex, featuring both coordination sites.

The structural characterization of all the compounds featured in Figure 2 reveal that they crystalize in the monoclinic $P2_1/c$ space group. This analysis evidenced only structural trait, differentiating two groups; the coordination mode of the nitrate ligand, which transits from bidentate for the lightest ions (from La to Eu) to monodentate for the heaviest ones (from Gd to Lu). Therefore, both sites of the [LnLn] molecules exhibit coordination number 9, unless when the NO_3^- ligand is chelating, which imposes coordination number 10. The different coordination environment for Ln1 and Ln2 was analysed by means of continuous shape measures (CShMs). While non-ideal polyhedron describes properly the environment of Ln1, the geometry for Ln2 was found close to either a spherical capped antiprism or a spherical tricapped trigonal prism. Moreover, the structural analyses for all homometallic [LnLn] compounds evidenced systematic longer Ln2-O bonds compared the Ln1-O ones (Figure 2). The parameter ΔO served to assess this property (ΔO difference between average distances of Ln2-O and Ln1-O, Table 1). This striking feature, which was exploited to promote access to heterometallic molecules (see below), contributed as well to the difference between both 4f ions in the molecular scaffold. The interaction between Ln1 and Ln2 was evaluated with molar magnetic susceptibility (χ) measurements on the paramagnetic analogues. The decline of the magnetic response when cooling the samples showed the expected depopulation of the excited Stark sublevels of the corresponding $^{2S+1}L_J$ multiplet, as well as a weak antiferromagnetic interaction between the metal ions.[52] The latter was assessed for both [GdGd] analogues (X = Cl^- and NO_3^-), which allows modelling the corresponding χ versus T dependence using the simple spin-only Hamiltonian $H = -JS_1S_2$ thanks to the lack of orbital angular momentum of Gd(III). The best fit J values (-0.02 and -0.04 cm^{-1} for chloride[56] and nitrate[52]

analogues, respectively) confirmed the proposed weak antiferromagnetic interaction, suggesting these homometallic [LnLn] molecules as ideal platforms for molecular quantum processors.

Site-selective one-pot formation of heterometallic [LnLn'] molecules

The structural characterization of the homometallic [LnLn] series demonstrated, not only different coordination environments between Ln1 and Ln2, but also a systematic difference of cavity size. As observed in Figure 2, the space available to Ln2 is larger than to Ln1. Thus, the molecular scaffold suggests a preference for larger metal ions in site 2, compared to site 1. This feature was exploited to create site-selective [LnLn'] molecules by following the same reaction procedure but using two different lanthanide ions together with H_3LA.[53, 57-59] The crystalline products obtained from these reactions were characterized both in solid state and in solution. The different combinations reported so far are listed in Table 1. The structural characterization served to confirm the heterometallic nature of these dinuclear derivatives, formulated as $(Hpy)[LnLn'(HLA)_3(NO_3)(py)H_2O]$ ([LnLn']). This extensive analysis demonstrated the preference of site 2 for encapsulating the lightest (largest) Ln ion, favouring the heaviest (smallest) one to occupy site 1. This feature was illustrated through the complete assessment of the [LnPr] series, which features the Pr^{III} ion together in this molecular architecture with each available Ln.[58] The structural study evidenced the preferential position of Pr^{III} depending on the accompanying partner. Thus, when combined with larger Ln ions (La^{III} and Ce^{III}), praseodymium is encapsulated in site 1 with av. *d*(Pr-O) of 2.47 Å, suited to promote shorter Ln-O bonds. However, when Ln is heavier (smaller ionic radii) than Pr^{III}, the latter switches to the larger cavity produced in site 2. This is corroborated with the analysis of av. *d*(Pr-O), which remain virtually constant at 2.50 Å (Figure 3) for the eleven molecules of this second group. In contrast, av. *d*(Ln1-O) drops from 2.46 Å for [PrPr] to 2.34 Å for [PrLu], in agreement with the contraction of Ln along the series in the parameters of site 1.

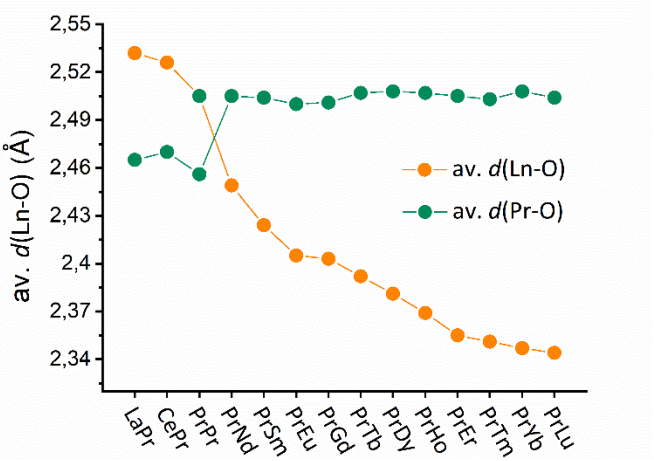

Figure 3. Plot of the average of Ln-O bond distances for all heterometallic $(Hpy)[LnPr(HLA)_3(NO_3)(py)H_2O]$ compounds considering only O atoms from HLA^{2-} ligands. The values for av. d(Pr-O) and av. d(Ln-O) are shown in green and orange, respectively.

For almost all binary combinations explored, the best refinement solution of the structural data converges to the expected distribution. The solutions obtained for other metallic distributions produce an increment to the refinement parameters R_1 and wR_2 (Table 1). The only analogues where the nature of Ln1 and Ln2 could not be clearly evidenced crystallographically derive from reactions involving Ln ions with ionic radii differences (Δr) smaller than 0.05 Å. As expected (Figure 3), the values of ΔO are correlated with Δr, increasing among the cases studied, from 0.02 Å for [CePr] (Δr = 0.02 Å) to 0.18 Å for [LaEr] (Δr = 0.21 Å). The site selective selectivity seems thus clearly related with difference in ionic radii of the metals combined. The unprecedented selectivity of the present molecular architecture was evaluated by electrospray ionization mass spectrometry (ESI-MS), using solutions in a mixture of MeOH and DMSO. As expected, for all compounds, signals corresponding to the heterometallic $[LnLn'(HLA)_2(H_2LA)]^+$ are predominant. Systems featuring lanthanide ions with significant different ionic radii show virtually no evidence of other Ln distributions. The spectrograms from the [LaGd] and [PrTm] derivatives are shown in Figure 4, illustrating the purity of the compounds. However, signals from the corresponding [LnLn] and [Ln'Ln'] homometallic analogues may be observed for compounds featuring ions with very similar sizes. These results are a reflect of a relaxation of the selectivity of the system in solution, which causes the marginal detection of non-heterometallic signals for some pairs with moderately higher Δr values (Table 1). Scrambling upon dissolution, as suggested by these observations study was corroborated by means of DFT calculations, which concluded a decrease on the selectivity derived from the loss of the terminal NO_3^-, H_2O and py ligands.[57]

Table 1. Structural parameters for all the reported (Hpy)[LnLn'(HL1)$_3$X(py)(H$_2$O)] analogues (X = Cl^- or NO_3^-).

[LnLn']	reference	anion	Δr (Å)[a]	av.Ln1-O (Å)[b]	av.Ln2-O (Å)[b]	ΔO (Å)	ΔR_1 (%)[c]	ΔwR_2 (%)[c]	$MS_{Scramb.}$[d]
[LaLa]	52	NO_3^-	-	2.500(18)	2.545(18)	0.05	-	-	-
[CeCe]	52	NO_3^-	-	2.480(21)	2.523(23)	0.04	-	-	-
[PrPr]	52	NO_3^-	-	2.457(18)	2.505(18)	0.05	-	-	-
[NdNd]	52	NO_3^-	-	2.445(25)	2.495(25)	0.05	-	-	-
[SmSm]	52	NO_3^-	-	2.413(57)	2.468(55)	0.06	-	-	-
[EuEu]	50	NO_3^-	-	2.405(29)	2.458(29)	0.05	-	-	-
[GdGd]	52	NO_3^-	-	2.405(64)	2.430(60)	0.03	-	-	-
[GdGd]	50	Cl^-	-	2.398(13)	2.452(14)	0.05	-	-	-
[TbTb]	52	NO_3^-	-	2.393(66)	2.427(61)	0.03	-	-	-
[TbTb]	50	Cl^-	-	2.372(42)	2.433(41)	0.06	-	-	-
[DyDy]	52	NO_3^-	-	2.370(53)	2.412(53)	0.04	-	-	-
[HoHo]	52	NO_3^-	-	2.360(30)	2.403(30)	0.04	-	-	-
[ErEr]	52	NO_3^-	-	2.353(28)	2.393(26)	0.04	-	-	-
[TmTm]	52	NO_3^-	-	2.342(26)	2.393(25)	0.05	-	-	-
[YbYb]	52	NO_3^-	-	2.340(45)	2.378(42)	0.04	-	-	-
[YY]	52	NO_3^-	-	2.343(88)	2.378(84)	0.04	-	-	-
[CePr]	60	NO_3^-	0.02	2.470(29)	2.525(28)	0.06	−0.22	−0.38	significant
[PrNd]	60	NO_3^-	0.03	2.448(18)	2.505(18)	0.06	−0.42	−2.94	significant
[LaPr]	60	NO_3^-	0.05	2.465(47)	2.533(44)	0.07	−0.38	−1.33	significant
[PrSm]	61	NO_3^-	0.06	2.423(18)	2.503(18)	0.08	3.52	4.20	significant
[PrEu]	60	NO_3^-	0.08	2.405(11)	2.500(11)	0.10	12.6	20.9	significant
[PrGd]	60	NO_3^-	0.10	2.403(22)	2.500(23)	0.10	7.99	14.4	significant
[GdYb]	62	NO_3^-	0.10	2.343(29)	2.417(29)	0.07	3.00	4.36	significant
[EuYb]	62	NO_3^-	0.11	2.353(35)	2.437(34)	0.08	2.99	5.00	significant
[PrTb]	60	NO_3^-	0.11	2.392(18)	2.507(18)	0.12	13.9	14.8	significant
[GdLu]	63	NO_3^-	0.11	2.342(58)	2.432(59)	0.09	1.34	2.24	significant
[PrDy]	60	NO_3^-	0.13	2.380(12)	2.508(12)	0.13	59.8	40.8	residual
[EuLu]	62	NO_3^-	0.13	2.340(18)	2.432(18)	0.09	13.4	20.6	significant
[CeGd]	61	NO_3^-	0.15	2.407(12)	2.527(12)	0.12	21.7	27.3	residual
[PrHo]	60	NO_3^-	0.15	2.368(30)	2.507(30)	0.14	11.4	12.8	residual
[LaGd]	63	NO_3^-	0.15	2.405(15)	2.535(16)	0.13	29.8	36.9	none
[PrEr]	60	NO_3^-	0.16	2.355(12)	2.505(12)	0.15	46.0	35.6	residual
[CeY]	53	NO_3^-	0.17	2.365(35)	2.517(35)	0.15	66.7	73.00	none
[NdYb]	62	NO_3^-	0.17	2.358(30)	2.492(30)	0.13	12.3	11.0	none
[NdLu]	62	NO_3^-	0.18	2.360(40)	2.492(38)	0.13	15.1	16.3	none
[CeEr]	53	NO_3^-	0.18	2.363(31)	2.530(30)	0.17	22.8	31.8	none
[PrTm]	60	NO_3^-	0.18	2.350(18)	2.503(18)	0.15	33.8	40.7	none
[PrYb]	60	NO_3^-	0.19	2.347(21)	2.508(20)	0.16	26.5	30.4	residual
[LaY]	53	NO_3^-	0.20	2.370(49)	2.547(53)	0.18	39.1	53.4	none
[PrLu]	60	NO_3^-	0.21	2.343(30)	2.503(31)	0.16	20.5	24.8	none
[LaEr]	53	NO_3^-	0.21	2.362(41)	2.543(42)	0.18	13.6	10	none

[a] Ionic radii values.[64]

[b] Only oxygen atoms from chelating HLA^{2-} ligands considered.

[c] Increase of percentage obtained by comparing with the values for the metal distribution producing the second best refinement parameters.

[d] Solution metal scrambling as detected by the appearance of [LnLn] fragments in the MS. "Significant" is a case where the [LnLn']/[LnLn] ratio of the corresponding signal maxima is larger than 0.78/0.22, whereas ratios below this number are considered as "residual" scrambling.

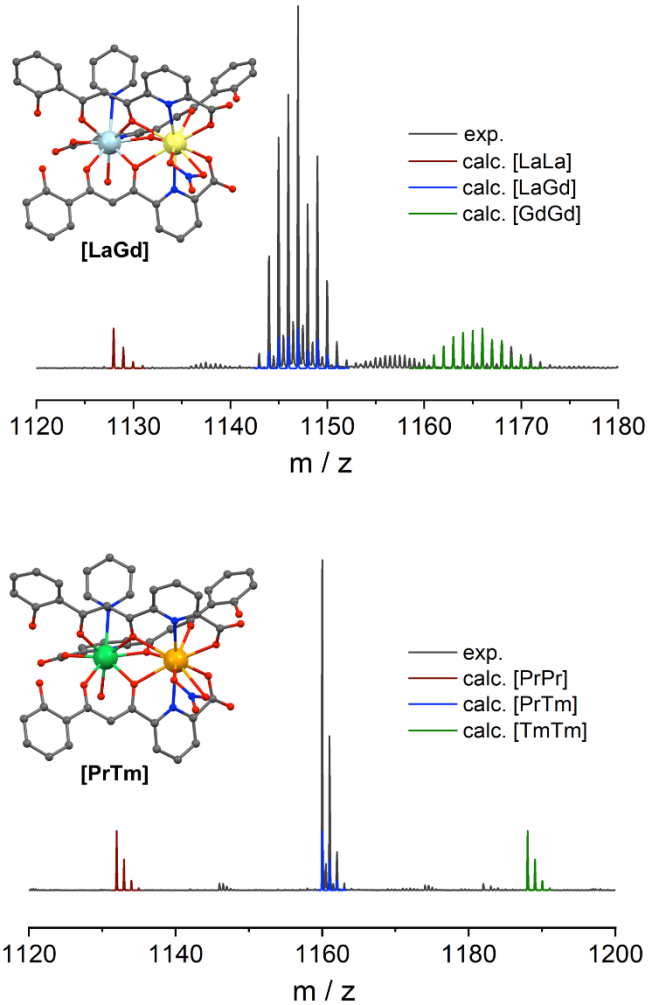

Figure 4. Crystal structure and selected region of the experimental (black line) ESI-MS spectra of [LaGd] and [PrTm], together with the calculated signals corresponding to the possible homometallic analogues.

Further information on the heterometallic nature of the [LnLn'] family was extracted from photophysical measurements on the analogues [EuYb] and [EuLu] in MeOH solution.[59] Interestingly, the emission of these compounds was satisfactorily ascribed to one unique Ln site, despite that they exhibit scrambling by mass spectrometry. These results evidenced the drastic effect of DMSO on the stability of the molecular scaffold, and thus in the process of scrambling in solution. The cumulative evidence thus indicates that the amount of pure [LnLn'] derivatives accessible by this chemical approach is noteworthy, thus providing numerous possible [LnLn'] analogues for embedding quantum bits and performing quantum logical operations. Notably, few other molecular architectures promoting one-pot heterometallic Ln-based compounds have been reported. As an example, an hexadentate ditopic ligand combining a benzimidazole-pyridine-carboxamide unit and a bis(benzimidazole)pyridine moiety was found to encapsulate two different Ln ions with selectivity up to 90 % based on ESI-MS and ^{1}H NMR studies, only for the most favourable cases.[65, 66] There are also examples of heterotrinuclear systems obtained with a tris-tridentate ligand, although with much decreased selectivity.[66] Interestingly, a quinolate ligand was used to produce trinuclear molecules with different metallic environments, thus favouring nonstatistical distributions of three different Ln ions. The selectivity, however, was very low.[67-69] The alternative way to obtain heterometallic compounds of high site-selectivity is through consecutive synthetic steps, thus sequentially positioning each Ln ion.[70-75] This strategy allows involves also binding two or more Ln discrete compounds, thus obtaining multinuclear complexes featuring two[76, 77] or three[78, 79] different 4f ions. The main drawback of these methods is that they are tedious and challenging synthetically, preventing the screening of many Ln combinations, the production of sufficient amounts for physical studies or implementations, the preparation of magnetically dilute materials or repeated attempts to grow large single crystals.

Realisation of quantum logical operations inside the [LnLn'] molecular architecture

The structural characterization of the different [LnLn'] analogues evidenced the potential of this unique molecular scaffold to embed two Ln-based quantum bits. The molecules provide great versatility for "*g* engineering" by allowing to choose in great measure the nature of both ions, ensuring magnetic dissymmetry even for the homometallic derivatives. In addition, they promote weak magnetic coupling among both metal ions. The controlled encapsulation of two different Ln ions, offers a versatility that is very useful for other purposes. For example, it allows studying full or partial diamagnetic analogues, and thus characterizing each qubit separately in the same environment exhibited in the corresponding two-qubit molecule. In the following sections, the potential shown by the [TbTb], [CeEr], [LaGd], [GdLu] and [GdGd] analogues as molecular prototypes for embedding quantum bits and universal quantum gates is revised.

Dinuclear lanthanide compounds for spin-based CNOT and SWAP quantum gates

As previously discussed, the low-lying magnetic states of a lanthanide ion can provide a good realization of the spin quantum bit. In general, the crystal field imposes a well-isolated ground state doublet, so that its $\pm m_J$ states can be used as the two-level (effective S = ½ spin) system to encode the qubit basis states defined by the spin up, $|1\rangle$ or spin down, $|0\rangle$ (Figure 5). Electromagnetic pulses can be then used to prepare quantum superpositions of those qubits. If several qubits are embedded in none molecule and conditional rotations of any of these are possible using also pulse sequences, these molecules may be used to implement multi-qubit qugates (see above).[25, 26] Considering the magnetic inequivalence of both lanthanide ions in the above described dinuclear complexes and their weak coupling, four non-degenerated Zeeman states originate under an external magnetic field, featuring unequal energy separations. This allows selecting the proper transitions in order to promote specifically either the CNOT or the SWAP operation, as shown in Figure 5.

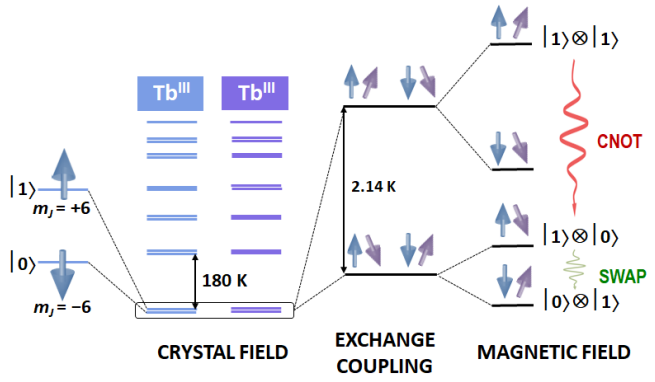

Figure 5. Qualitative energy level splitting derived from the crystal field, exchange coupling and magnetic field effect for [TbTb]. The two states of the spin qubit (spin up as |1⟩, and spin down as |0⟩) as well as the CNOT and SWAP operations are shown.

The homometallic [TbTb] analogue (X = Cl^-, Figure 6) was investigated down to sub-Kelvin temperatures to confirm this strategy.[51] The χT *vs* T plot showed a drop below 100 K that was ascribed to the depopulation of the excited Stark sublevels derived from the crystal field (Figure 6). From this data, an approximate value for the uniaxial anisotropy D was determined, which allowed estimating a separation between the ground state and the first excited state of 180 K and thus ensuring a well-isolated doublet for each of the Tb ions (Figure 5). The second drop observed below 3 K can be attributed to the antiferromagnetic coupling between the two Tb qubits, which was corroborated by magnetic heat capacity measurements. Interestingly, a finite magnetic moment is observed despite the presence of such antiparallel exchange interaction, which can be modelled considering that the easy axes of each qubit are not parallel but tilted. A value of this tilting angle δ of 66° was found to reproduce satisfactorily both magnetic and heat capacity data. Most importantly, this model explains the magnetic asymmetry of the dinuclear entity, and thus the non-equivalence of the two spin qubits. In order to demonstrate that the system allows promoting the transitions associated to the logical operations, the energy level spectrum was generated by simulation (Figure 6). Continuous-wave EPR measurements were performed in frozen solutions in order to show that transitions between $|1\rangle \otimes |0\rangle$ and $|0\rangle \otimes |1\rangle$ (SWAP gate) or $|1\rangle \otimes |0\rangle$ and $|1\rangle \otimes |1\rangle$ (CNOT gate) can be carried out by selecting the required magnetic field where only those are resonant with X-band photons.

The study performed on [TbTb] demonstrated that the designed molecular scaffold meets the requirements to implement selected logical operations. In order to exploit their physical realization, and taking advantage of the chemical versatility of these compounds, the study was extended to the heterometallic analogue [CeEr], which offers several advantages.[53] The ions Ce^{III} and Er^{III} exhibit very different magnetic behaviour (J = 5/2 and g_J = 6/7 for the former and J = 15/2 and g_J = 6/5 for the latter). Also, since both are Kramer's ions, the crystal field interaction is expected to lead to doubly degenerated ground states, neatly isolated from the excited states. Moreover, the presence of magnetic nuclear spin is drastically reduced, carried only by 23 % of the stable isotopes for Er(III), thus contributing to reduce decoherence. The adaptability of the coordination architecture allowed studying each isolated Ln qubit by selecting, respectively, the [CeY] and [LaEr] analogues. These compounds exhibit both Ce^{III} and Er^{III} ions at the same position as in [CeEr], together with a diamagnetic ion (Y^{III} and La^{III}, respectively, Figure 7).

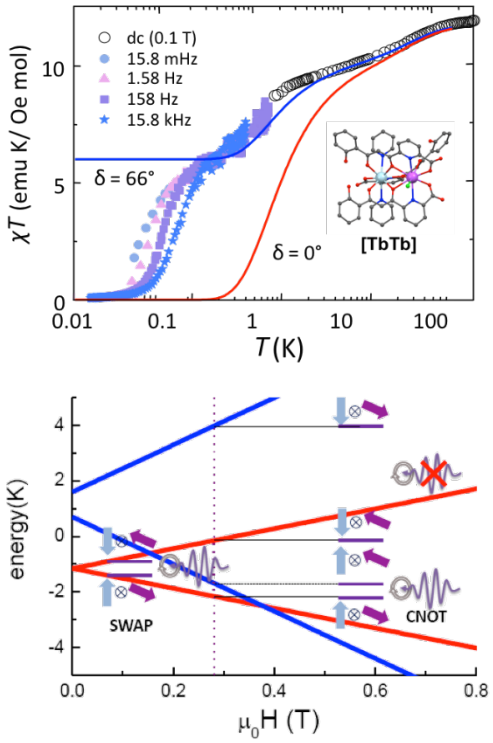

Figure 6. Top: dc and frequency dependent ac magnetic susceptibility data of [TbTb] at different frequencies. Solid lines are least square fits for collinear (δ = 0°, red) and noncollinear (δ = 66°, blue) anisotropy axes. Inset: Representation of the crystal structure of [TbTb]. Bottom: Field-dependent magnetic energy levels of [TbTb], showing the SWAP and CNOT operations. Adapted from reference [51].

Magnetic susceptibility and EPR data from these analogues were used to obtain information on the magnetic energy level structure and thus the nature of the ground state doublet for each Ln qubit. As expected, the effective gyromagnetic g_i tensors found for Ce^{III} and Er^{III} ions were very different, quantifying their magnetic inequivalence. Again, the first excited sublevel was found to be well above the ground state doublet, with a Δ_{Ln} energy difference of 43 and 230 K for Er^{III} and Ce^{III}, respectively (Figure 7). The physical characterization of [CeEr] allowed determining a weak antiferromagnetic coupling between both qubits, and thus again an optimal energy level diagram to promote two-qubit logical operations. In this case, the coherence of the resonance corresponding to the CNOT operation was examined by time-domain EPR spectroscopy. The echo signal detected was found to decay exponentially, providing a decoherence time of $T_M \approx 410$ ns (Figure 7) and demonstrating for the first time the feasibility of coherent manipulations on a two-qubit molecular spin quantum gate made using coordination chemistry.

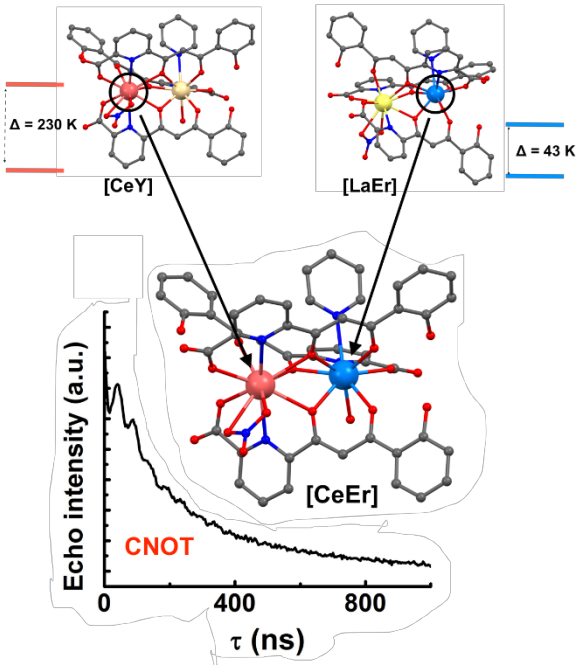

Figure 7. Top: representation of the crystal structure of [CeY], [LaEr] (with the corresponding zero field Δ energy difference between the ground state and first excited state doublets) and [CeEr], showing the controlled disposition of each Ln qubit in the [CeEr] molecular processor. Bottom: decay of the Echo intensity for the transition corresponding to the CNOT operation in [CeEr], from which T_M is estimated. Data taken from reference [53].

Exploiting the [LnLn'] coordination architecture to embed six addressable qubits

One of the main advantages of using lanthanides for quantum computation is the possibility to increase the number of spin qubits within the metal ion. As observed before for the [TbTb] or [CeEr] analogues, the isolated ground state $\pm m_J$ doublet of each Ln may be exploited to realize one quantum bit, thus allowing two-qubit quantum operations in these molecules. However, several quantum bits can be embedded in a single Ln ion if multiple spin levels are accessible. This would enable to increase the density of quantum information. In particular, the eight different m_J states produced by the S =7/2 spin state of Gd^{III} (which features no orbital angular momentum, *i.e.* L = 0) offer a unique energy level diagram to realize three quantum bits. Since the intrinsic anisotropy of this ion is negligible, its zero field splitting arises from the crystal field and thus from small distortions of the coordination environment. The transitions between the corresponding magnetic levels are, consequently, all accessible via conventional magnetic spectroscopic techniques. Our molecular platform can undoubtedly provide the required compounds to explore such strategy.[63] The heterometallic [LaGd] and [GdLu] analogues, for example, allowed characterizing the energy levels of Gd^{III} in the two available coordination positions (site 1 and site 2, Figure 8). Being accompanied by diamagnetic Ln partners, the properties of the isolated Gd^{III} ions were assessed by magnetic and spectroscopic measurements. Using continuous-wave EPR and heat capacity, the zero-field splitting parameters D and E were deduced, and found to be different from one metal to the other as expected from their different coordination environments (Figure 8). From these data, the energy level structure for each Gd^{III} ion was obtained. The coherence of various of the transitions within these manifolds was assessed by electron spin-echo decay studies in frozen solutions at different magnetic fields. The values of T_M obtained (from 1.05 to 0.73 μs for [LaGd] and from 1.31 to 0.85 μs for [GdLu], respectively) confirmed both compounds as potential three-qubit molecular platforms.

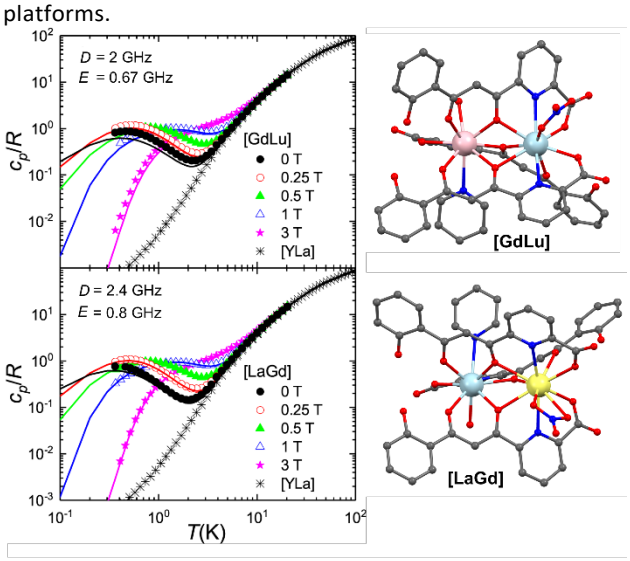

Figure 8. Left: Magnetic heat capacity measurements performed on [GdLu] and [LaGd] at zero and different applied magnetic fields. Solid lines are numerical calculations using the indicated D and E parameters obtained from EPR data. Right: Crystal structures of both analogues. Adapted from reference [63].

In order to explore the system with both sites incorporating Gd^{III}, the homometallic [GdGd] analogue was assessed (Figure 9). Considering the presence of magnetic coupling between both ions, 64 unequally spaced energy levels can be generated, thus codifying six qubits (all combinations from $|000000\rangle$ to $|111111\rangle$). The physical characterization of [GdGd] evidenced an antiferromagnetic interaction in the compound, and thus the confirmation of such energy diagram (Figure 9). In this case, the coherence for transitions between some of those levels was found to be slightly reduced (T_M = 0.73 μs, virtually constant for the fields explores), suggesting the interaction between both ions as a source of decoherence. Nevertheless, the experiments performed on the three systems confirmed that hyperfine interactions with solvent molecules are the main influence on T_M. This study underscores the possibility to increase the number of accessible quantum bits in the molecular platform, and thus the potential of this chemical approach for quantum technology with higher performance. However, one major drawback to overcome is the fact that the energy diagram hosting the computational basis becomes excessively crowded for individual addressing (as is evident in Figure 9). The alternative approach to attain higher complexity is the increase of the number of metals acting as individual addressable qubits within the molecule.

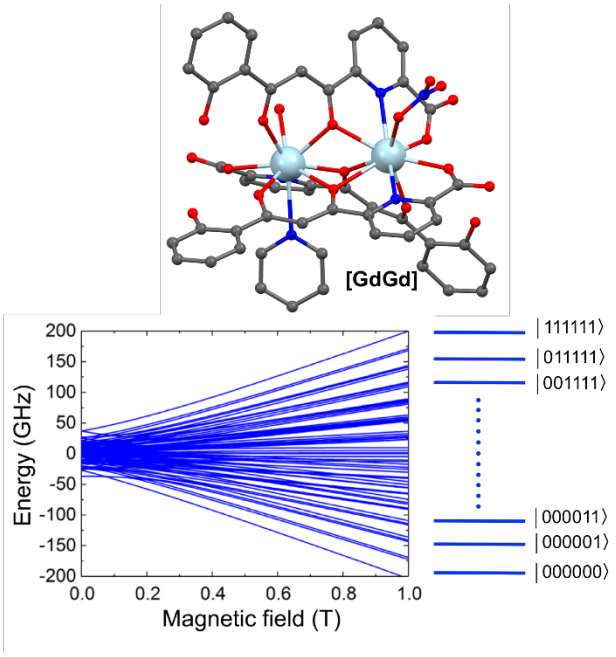

Figure 9. Top: Molecular structure of [GdGd], featuring both type of Gd^{III} ions. Bottom: Energy level diagram for [GdGd], featuring the non-equivalent 64 levels, together with the possible labelling in terms of the basis states of six qubits. Adapted from reference [63].

Increasing the complexity: Ligand-based strategy to encapsulate three Ln qubits

The discovery of the highly performant [LnLn'] system unveiled a synthetic avenue for the preparation of novel families of coordination chemistry molecules featuring site-selective hetero-lanthanide composition. In H_3LA, the two different chelating units, β-diketone (O,O) and dipicolinate-like (O,N,O), directly influence the preference for Ln ions with smaller or larger radii, respectively. Following on this principle, we decided to explore the coordination capabilities of the ligand H_2LB, featuring an additional β-diketone unit (Scheme 1).[80] By analogy with H_3LA, this organic molecule could potentially incorporate three Ln ions while keeping the two-metal selectivity. In that sense, the central dipicolinate-like (O,N,O) group was to allocate the largest Ln ion, while Ln featuring smaller ionic radii would be chelated in both diketonate units. The realization of these trinuclear [LnLn'Ln] heterometallic compounds would allow studying a molecular system with three Ln qubits and thus realizing more complex quantum operations, such as quantum error correction protocols (see below).

As previously seen for [LnLn'], mixing H_2LB with two different $Ln(NO_3)_3$ salts in pyridine through one-pot reactions produced the expected [LnLn'Ln] trinuclear entities. The different Ln/Ln' combinations reported so far are shown in Table 2. As observed from their crystal structure, in all cases the molecule exhibits three lanthanide ions chelated in this case by four ligands (Figure 10). Interestingly, two of the ligands are the result of partial in-situ hydrolysis, one β-diketone group being converted to a carboxylic acid (H_2LC, Scheme 1). Together with this new ligand, the structural characterization revealed the exact nature of these heterometallic and heteroleptic complexes with formula $[Ln_2Ln'(LB)_2(LC)_2(py)(H_2O)_2](NO_3)$ ([LnLn'Ln]). The stoichiometric synthesis of the compounds from their components was carried out by producing the ligand H_2LC and conducting the corresponding reactions. Interestingly, in this case, the difference in coordination environment is even more severe than in the [LnLn'] system. The central Ln2 ion is undeca-coordinated, with two dipicolinate-like (O,N,O) units, two diketonate (O,O) groups and one pyridine ligand. The peripheral Ln1 ions are, in contrast, octa-coordinated, featuring two diketonate groups, one dipicolinate-like unit and one molecule of water. The positive charge of the resuting cationic species is compensated with a nitrate anion in the crystal lattice. The identity of each lanthanide ion was clearly evidenced by the refinement of the corresponding crystal structures, since other metallic distributions produced significant worst parameters (Table 2). As observed for [LnLn'], the analysis of bond lengths corroborated the selectivity of the molecular architecture, since larger values were observed for the average value of Ln2-O when compared to the coordination bonds for both Ln1 ions. As expected, the difference between both sites (ΔO) was found to depend on Δr, obtaining higher values for larger differences of ionic radii. This metric parameter also suggested the much higher difference between coordination cavities in the trinuclear molecular scaffold when compared to [LnLn']. The dinuclear analogues [CeEr] and [LaEr], for example, have values of ΔO = 0.17 and 0.18 Å, respectively, while those for the corresponding [ErCeEr] and [ErLaEr] compounds are almost twofold larger (0.30 and 0.32 Å, respectively). The enhanced lanthanide selectivity was also transferred in solution. ESI mass spectrometry measurements performed under the same conditions as for [LnLn'] showed signals corresponding exclusively to the [LnLn'Ln] metal distribution for all the analogues studied to date, with no evidence of scrambling (Figure 11). These results demonstrated the success of the ligand-based strategy to control the disposition of three lanthanide ions in a molecule through one-pot reactions, and thus the possibility to explore its potential for new molecular quantum processors.

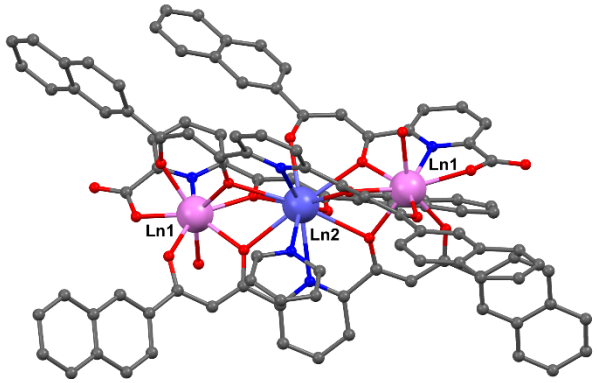

Figure 10. Representation of the characteristic molecular structure of the [LnLn'Ln] series, taken from the crystal structure of $[Ln_2Ln'(LB)_2(LC)_2(py)(H_2O)_2](NO_3)$ (Ln1 = Er, Ln2 = Er). The nitrate anion, as well as the H atoms, have been omitted for clarity. C, N and O atoms are shown in grey, blue and red, respectively.

ARTICLE

Table 2. Structural parameters for the reported $[Ln_2Ln'(LB)_2(LC)_2(py)(H_2O)_2](NO_3)$ analogues.

[LnLn'Ln]	*reference*	Δ*r* (Å)[a]	*av*.Ln1-O (Å)[b]	*av*.Ln2-O (Å)[b]	ΔO (Å)	ΔwR_1 (%)[c]	ΔwR_2 (%)[c]	$MS_{Scramb.}$[d]
[HoCeHo]	CEJ 2019	0.17	2.344(23) / 2.335(23)	2.622(30)	0.28 / 0.30	23.0	31.6	None
[ErCeEr]	CEJ 2019	0.18	2.323(23) / 2.325(23)	2.622(31)	0.30 / 0.30	30.7	39.7	None
[ErLaEr]	CS 2020	0.21	2.334(81) / 2.322(81)	2.628(107)	0.30 / 0.31	6.57	8.68	None
[YbCeYb]	CEJ 2019	0.21	2.301(33) / 2.303(33)	2.614(43)	0.31 / 0.31	20.6	25.5	None
[LuCeLu]	CS 2020	0.23	2.298(24) / 2.294(24)	2.615(32)	0.32 / 0.32	41.0	51.3	None

[a] Ionic radii values obtained from D'Angelo et al.[64]

[b] Only oxygen atoms from chelating LB^{2-} and LC^{2-} ligands were considered.

[c] Increase of percentage obtained by comparing with the values for the metal distribution producing the second best refinement parameters.

[d] Solution metal scrambling as detected by the appearance of [LnLn] fragments in the MS. "Significant" is a case where the [LnLn']/[LnLn] ratio of the corresponding signal maxima is larger than 0.78/0.22, whereas ratios below this number are considered as "residual" scrambling.

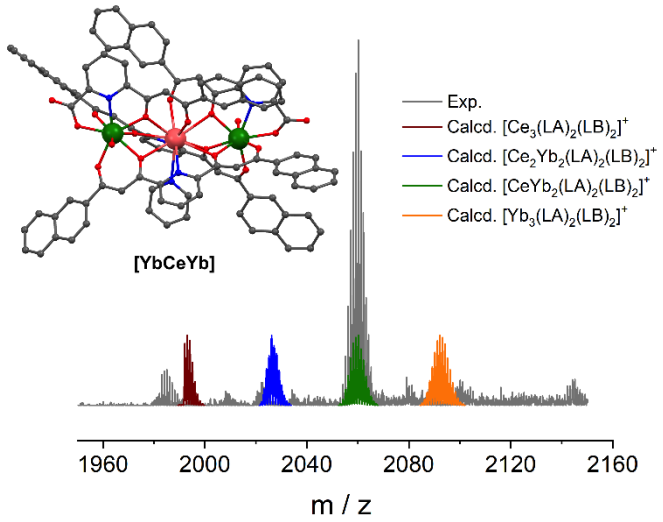

Figure 11. Crystal structure of [YbCeYb] and selected region of its experimental (black line) ESI-MS spectrum, together with the calculated signals corresponding to the possible homometallic analogues. Adapted from reference [80].

Complexes [LnLn'Ln] as three-qubit molecular processors: Implementing quantum error correction

One of the main concerns regarding QIP is the fragility of the quantum information conveyed by qubits, since their superposition states can be easily altered due to interactions with the environment. Protocols for quantum error correction (QEC) must be therefore developed for ensuring the proper realization of quantum operations.[81] These protocols may become extremely simplified if they can be performed by conditional operations on three addressable qubits connected to each other. In this protocol, two auxiliary qubits are used to protect an encoded qubit from phase flips (the most significant source of decoherence in molecular magnets).[82] This is carried out following consecutive operations on these three quantum bits, known as three-qubit phase-flip repetition code, in three different stages. The first step (*encoding*) consists of two CNOT operations between the qubit carrying the logical information (central qubit) and each of the two auxiliary qubits initialized into the $|0\rangle$ state. Together with a $\pi/2$ rotation on the three qubits, these operations bring the encoded qubit into a state protected from phase flips, and thus robust against dephasing. The three qubits are left undisturbed during a *memory time* τ, where their evolution depends only on pure dephasing. Then, the same gates from the *encoding* step are carried out in reverse order ($\pi/2$ rotations and CNOT operations) thus producing the *decoding* step. The final step is the *correction* one, consisting of a controlled-controlled-NOT operation (CCNOT) where the (central) qubit is the target and the ancillae are the control qubits. If there has been an error, this step corrects it. In order to promote these operations, the molecular architecture must consequently exhibit three addressable weakly coupled effective S = ½ ions. The trinuclear [LnLn'Ln] compound perfectly fulfils these requirements, in particular those analogues featuring anisotropic lanthanide ions with well-isolated ground states. The inequality between the distal qubits is ensured by their different respond to a magnetic field, since they have their anisotropy axes oriented differently. In order to study and implement the correction code, [ErCeEr] was chosen, Ce^{III} being the encoded qubit and the two Er^{III} ions acting as auxiliary qubits.[83] The complex was thus magnetically and spectroscopically characterized, together with the analogues [ErLaEr] and [LuCeLu], which allow studying each type of Ln qubit individually. The experimental data obtained from the latter allowed determining the corresponding g tensors, obtaining best values of g_{Ce} = (1.7, 1.7, 2.2) and g_{Er} = (1, 2, 11.5). Measurements performed on [ErCeEr] were then used to assess the Er-Ce interaction, providing dipole-dipole interaction tensors of J_{ErCe} = (0.01, 0.07, -0.29) cm^{-1} and J_{ErEr} = (0.00, 0.02, -0,22) cm^{-1}. The results clearly demonstrated the ability of [ErCeEr] to promote the correction code, since it showed the existence of spin-spin interactions, and indicated a large and highly anisotropic g tensor for erbium, significantly different from that of cerium, while the three qubits being addressable.

From the whole set of data, the level diagram for the three interacting qubits was determined, showing that specific transitions between each of the magnetic energy levels can be driven by means of microwave resonant pulses (Figure 12). Thus, each CNOT operation can be implemented a different pulse. The $CNOT_{2\to3}$ (targeting the third qubit, Er^{III}, controlled by the central Ce^{III} ion), for example, is promoted by transitions between $|110\rangle$ and $|111\rangle$ states, and between $|010\rangle$ and $|011\rangle$. $\pi/2$ rotations require four pulses of slightly different frequencies, while CCNOT gate can be performed by a single pulse resonant with the $|101\rangle \leftrightarrow |111\rangle$ transition. Pulsed EPR measurements allowed assessing the phase memory time T_M at different fields where the transitions of interest take place, yielding values close to 0.5 μs. Time-dependent numerical simulations were then performed in order to demonstrate the viability of the protocol. From these, the difference between the initial stored logical state $|\psi\rangle$ and the corrected or uncorrected state of the Ce^{III} qubit were assessed. The simulations evidenced that the error is efficiently reduced by the correction code, allowing the implementation of 50-100 logical gates before its repetition becomes necessary. The results thus evidenced the possibility of exploiting such Ln-based molecules not only to encode qubits but also to embed quantum error correction.

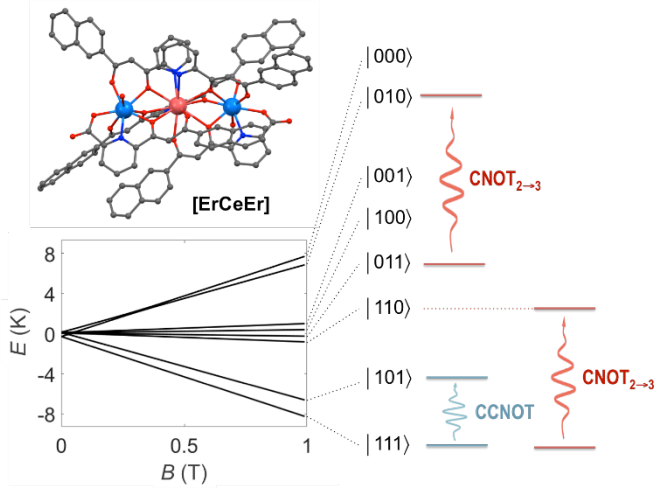

Figure 12. Crystal structure of [ErCeEr] and energy levels as a function of the external magnetic field, *B*, applied along z (the Er-Ce direction). The qubits states for the eight levels are depicted, together with the transitions corresponding to the $CNOT_{2\to3}$ and CCNOT quantum gates. Adapted from reference [83].

Conclusions and outlook

This perspective has outlined a novel and very promising synthetic strategy to prepare site-selective heterometallic lanthanide molecules of different nuclearity, through ligand design, based on atomic radii differences. The different polynuclear Ln compounds revised here highlight the ability of specifically targeted systems for certain quantum logic operations. Thus, by combining two different chelating units such a diketonate and dipicolinate-like groups, different cavities can be promoted in a molecular scaffold, providing different environments (and physical properties) to the corresponding Ln qubits. Undoubtedly, this synthetic approach is very promising, since new original architectures can be designed exploiting and tuning organic ligands. As an example, the dinuclear [LnLn'] molecular system has been accessed from partially deprotonated HLA^{2-} ligands, leaving the phenol group unaltered. However, as carried out for similar ligands, the latter could be further deprotonated under stronger basic conditions, thus promoting an additional "diketonate" pocket and potentially larger nuclearity.[84] On the other side, new asymmetric ligands featuring additional dipicolinate-like units could promote a third chemical environment in the molecular scaffold. As it has been observed, both [LnLn'] and [LnLn'Ln] compounds adopt larger Ln ions in cavities exhibiting higher number of dipicolinate-like groups. Through this approach one can imagine, for example, selectively locating three different types of 4f ions discriminated by their size, producing heterotrimetallic entities directly through one-pot reactions. On that respect, the use of similar chelating units, such as picolinate moieties, could also promote additional different coordination environments.[85]

On the other hand, and despite the potential of molecular design, it should be pointed out that for molecules to perform quantum logical operations, a crucial step must be made: the integration of these spin-based quantum material into a technological device to allow writing, processing and reading-out the information. In this regard, an appealing proposal is based on the design of new hybrid devices by coupling individual molecules with superconducting coplanar resonators and transmission lines.[86] The device is based on a coplanar superconducting resonator where the molecules are deposited near superconducting wave-guides. The former and the latter are responsible for creating general and local magnetic fields, which can be taken in and out-of resonance with a specific molecular entity to perform a quantum operation. In order to accomplish these hybrid devices, considered as the last step for controlling and communicating the information of the molecules, further specific considerations should be taken into account regarding the molecular design. Aside from embedding magnetically inequivalent and weakly coupled Ln ions, the molecular entities must be robust to permit their deposition. In this respect, both [LnLn'] and [LnLn'Ln] complexes have shown great stability in solution, opening the possibility to be exploited *via* deposition using the proposed DIP-Pen nanolithography.[86] Additionally, the interaction of the molecules with the surface must be sufficiently strong, and with a preferred orientation, to ensure homogeneous coupling. In that sense, additional grafting groups could be incorporated into the corresponding organic ligands of the Ln molecules. Considering the two addressable surfaces used for the hybrid quantum processor (metallic Nb or Si/SiO_2), several possibilities might be explored. Metallic surfaces could be, for example, exploited with molecules featuring thiol or aromatic groups, while the addition of carboxylate or phosphonate groups could be used to allow deposition of the molecule over oxide-based surfaces. The design of Ln systems thus drifts to a laborious but very attractive challenge for synthetic coordination chemists devoted to construct the future devices for QIP.

Conflicts of interest

The authors declare no conflicts of interest.

Acknowledgements

The authors thank the European Union's Horizon 2020 research and innovation programmes QUANTERA project SUMO and FET-OPEN grant 862893 FATMOLS (GA and OR) the Spanish MICINN for grants PGC2018-098630-B-I00 (GA and DA) and MAT2017-86826-R (OR) and the Generalitat de Catalunya for the ICREA Academia 2018 Prize (GA).

Notes and references

1. C. P. Montgomery, B. S. Murray, E. J. New, R. Pal and D. Parker, *Accounts of Chemical Research* 2009, **42**, 925-937.
2. C.-H. Huang, *Rare earth coordination chemistry*, Wiley, Singapore, 2010.
3. S. V. Eliseeva and J.-C. G. Bünzli, *New J. Chem.* 2011, **35**, 1165-1176.
4. A. de Bettencourt-Dias, *Luminescence of lanthanide ions in coordination compounds and nanomaterials*, Wiley, Chichester, U.K., 2014.
5. R. A. Layfield and M. Murugesu, *Lanthanides and Actinides in Molecular Magnetism*, Wiley-VCH, Weinhem, Germany, 2015.
6. *Recent Development in Clusters of Rare Earths and Actinides: Chemistry and Materials*, Springer-Verlag Berlin Heidelberg, Berlin, Germani, 2017.
7. J.-C. G. Bünzli, *Eur. J. Inorg. Chem.* 2017, **2017**, 5058-5063.
8. *Lanthanide-Based Multifunctional Materials. From OLEDs to SIMs*, Elsevier, 2018.
9. J.-L. Liu, Y.-C. Chen and M.-L. Tong, *Chem. Soc. Rev.* 2018, **47**, 2431-2453.
10. O. Cador, B. Le Guennic and F. Pointillart, *Inorg. Chem. Front.* 2019, **6**, 3398-3417.
11. L. Ungur, in *Lanthanide-Based Multifunctional Materials*, eds. P. Martín-Ramos and M. Ramos Silva, Elsevier, 2018, DOI: https://doi.org/10.1016/B978-0-12-813840-3.00001-6, pp. 1-58.
12. G. H. Dieke, H. M. Crosswhite and H. Crosswhite, *Spectra and Energy Levels of Rare Earth Ions in Crystals*, Interscience Publishers, 1968.
13. R. Hull, J. Parisi, R. Osgood, H. Warlimont, G. Liu and B. Jacquier, *Spectroscopic Properties of Rare Earth in Optical Materials*, Springer, 2005.
14. J.-C. G. Bünzli, *Chem. Rev.* 2010, **110**, 2729-2755.
15. S. V. Eliseeva and J.-C. G. Bünzli, *Chem. Soc. Rev.* 2010, **39**, 189-227.
16. A. J. Amoroso and S. J. A. Pope, *Chem. Soc. Rev.* 2015, **44**, 4723-4742.
17. K. Jinnai, R. Kabe and C. Adachi, *Chem. Commun.* 2017, **53**, 5457-5460.
18. J. Kido and Y. Okamoto, *Chem. Rev.* 2002, **102**, 2357-2368.
19. L. Sorace and D. Gatteschi, in *Lanthanides and Actinides in Molecular Magnetism*, eds. R. Layfield and M. Murugesu, Wiley-VCH, 2015, DOI: 10.1002/9783527673476.ch1, pp. 1-26.
20. D. N. Woodruff, R. E. P. Winpenny and R. A. Layfield, *Chem. Rev.* 2013, **113**, 5110-5148.
21. F.-S. Guo, B. M. Day, Y.-C. Chen, M.-L. Tong, A. Mansikkamäki and R. A. Layfield, *Angew. Chem., Int. Ed.* 2017, **56**, 11445-11449.
22. C. A. P. Goodwin, F. Ortu, D. Reta, N. F. Chilton and D. P. Mills, *Nature* 2017, **548**, 439-442.
23. P. Zhang, L. Zhang and J. Tang, *Dalton Trans.* 2015, **44**, 3923-3929.
24. Z. Zhu, X.-L. Li, S. Liu and J. Tang, *Inorg. Chem. Front.* 2020, **7**, 3315-3326.
25. G. Aromí, F. Luis and O. Roubeau, in *Lanthanides and Actinides in Molecular Magnetism*, eds. R. A. Layfield and M. Murugesu, Wiley-WCH, 2015, DOI: doi:10.1002/9783527673476.ch7, pp. 185-221.
26. G. Aromí and O. Roubeau, in *Handbook on the Physics and Chemistry of Rare Earths*, eds. J.-C. G. Bünzli and V. K. Pecharsky, Elsevier, 2019, vol. 56, pp. 1-54.
27. J. Clarke and F. K. Wilhelm, *Nature* 2008, **453**, 1031-1042.
28. J. M. Gambetta, J. M. Chow and M. Steffen, *npj Quantum Information* 2017, **3**, 2.
29. M. Kjaergaard, M. E. Schwartz, J. Braumüller, P. Krantz, J. I. J. Wang, S. Gustavsson and W. D. Oliver, *Annu. Rev. Condens. Matter Phys.* 2020, **11**, 369-395.
30. J. M. Pino, J. M. Dreiling, C. Figgatt, J. P. Gaebler, S. A. Moses, M. S. Allman, C. H. Baldwin, M. Foss-Feig, D. Hayes, K. Mayer, C. Ryan-Anderson and B. Neyenhuis, *Nature* 2021, **592**, 209-213.
31. C. D. Bruzewicz, J. Chiaverini, R. McConnell and J. M. Sage, *Appl. Phys. Rev.* 2019, **6**, 021314.
32. S. Slussarenko and G. J. Pryde, *Appl. Phys. Rev.* 2019, **6**, 041303.
33. S. Takeuchi, *Proc. Jpn. Acad. Ser. B-Phys. Biol. Sci.* 2016, **92**, 29-43.
34. G. Aromí, D. Aguilà, P. Gamez, F. Luis and O. Roubeau, *Chem. Soc. Rev.* 2012, **41**, 537-546.
35. A. Ardavan, O. Rival, J. J. L. Morton, S. J. Blundell, A. M. Tyryshkin, G. A. Timco and R. E. P. Winpenny, *Phys. Rev. Lett.* 2007, **98**, 057201.
36. C. J. Wedge, G. A. Timco, E. T. Spielberg, R. E. George, F. Tuna, S. Rigby, E. J. L. McInnes, R. E. P. Winpenny, S. J. Blundell and A. Ardavan, *Phys. Rev. Lett.* 2012, **108**, 107204.
37. G. A. Timco, T. B. Faust, F. Tuna and R. E. P. Winpenny, *Chem. Soc. Rev.* 2011, **40**, 3067-3075.
38. J. Ferrando-Soria, E. Moreno Pineda, A. Chiesa, A. Fernandez, S. A. Magee, S. Carretta, P. Santini, I. J. Vitorica-Yrezabal, F. Tuna, G. A. Timco, E. J. L. McInnes and R. E. P. Winpenny, *Nature Commun.* 2016, **7**, 11377.
39. M. Warner, S. Din, I. S. Tupitsyn, G. W. Morley, A. M. Stoneham, J. A. Gardener, Z. L. Wu, A. J. Fisher, S. Heutz, C. W. M. Kay and G. Aeppli, *Nature* 2013, **503**, 504-508.
40. M. S. Fataftah, M. D. Krzyaniak, B. Vlaisavljevich, M. R. Wasielewski, J. M. Zadrozny and D. E. Freedman, *Chem. Sci.* 2019, **10**, 6707-6714.
41. K. Bader, D. Dengler, S. Lenz, B. Endeward, S.-D. Jiang, P. Neugebauer and J. Van Slageren, *Nature Commun.* 2014, **5**, 5304.
42. K. Bader, M. Winkler and J. van Slageren, *Chem. Commun.* 2016, **52**, 3623-3626.
43. M. Atzori, E. Morra, L. Tesi, A. Albino, M. Chiesa, L. Sorace and R. Sessoli, *J. Am. Chem. Soc.* 2016, **138**, 11234-11244.
44. M. Atzori, L. Tesi, E. Morra, M. Chiesa, L. Sorace and R. Sessoli, *J. Am. Chem. Soc.* 2016, **138**, 2154-2157.

45. M. D. Jenkins, Y. Duan, B. Diosdado, J. J. Garcia-Ripoll, A. Gaita-Arino, C. Gimenez-Saiz, P. J. Alonso, E. Coronado and F. Luis, *Phys. Rev. B* 2017, **95**, 064423.
46. G. Taran, E. Bonet and W. Wernsdorfer, *J. Appl. Phys.* 2019, **125**, 142903.
47. M. J. Martinez-Perez, S. Cardona-Serra, C. Schlegel, F. Moro, P. J. Alonso, H. Prima-Garcia, J. M. Clemente-Juan, M. Evangelisti, A. Gaita-Arino, J. Sese, J. van Slageren, E. Coronado and F. Luis, *Phys. Rev. Lett.* 2012, **108**, 247213.
48. K. S. Pedersen, A.-M. Ariciu, S. McAdams, H. Weihe, J. Bendix, F. Tuna and S. Piligkos, *J. Am. Chem. Soc.* 2016, **138**, 5801-5804.
49. M. Shiddiq, D. Komijani, Y. Duan, A. Gaita-Ariño, E. Coronado and S. Hill, *Nature* 2016, **531**, 348-351.
50. D. Aguila, L. A. Barrios, F. Luis, A. Repolles, O. Roubeau, S. J. Teat and G. Aromí, *Inorg. Chem.* 2010, **49**, 6784-6786.
51. F. Luis, A. Repollés, M. J. Martínez-Pérez, D. Aguilà, O. Roubeau, D. Zueco, P. J. Alonso, M. Evangelisti, A. Camon, J. Sese, L. A. Barrios and G. Aromí, *Phys. Rev. Lett.* 2011, **107**, 117203.
52. D. Aguilà, L. A. Barrios, V. Velasco, L. Arnedo, N. Aliaga-Alcalde, M. Menelaou, S. J. Teat, O. Roubeau, F. Luis and G. Aromí, *Chem., Eur. J.* 2013, **19**, 5881-5891.
53. D. Aguilà, L. A. Barrios, V. Velasco, O. Roubeau, A. Repollés, P. J. Alonso, J. Sesé, S. J. Teat, F. Luis and G. Aromí, *J. Am. Chem. Soc.* 2014, **136**, 14215-14222.
54. L. A. Barrios, E. Peyrecave-Lleixa, G. A. Craig, O. Roubeau, S. J. Teat and G. Aromí, *Eur. J. Inorg. Chem.* 2014, 6013-6021.
55. V. Velasco, L. A. Barrios, M. Schütze, O. Roubeau, F. Luis, S. J. Teat, D. Aguilà and G. Aromí, *Chem., Eur. J.* 2019, **25**, 15228 – 15232.
56. D. Aguilà, L. A. Barrios, F. Luis, A. Repollés, O. Roubeau, S. J. Teat and G. Aromí, *Inorg. Chem.* 2010, **49**, 6784-6786.
57. J. Gónzalez-Fabra, N. A. G. Bandeira, V. Velasco, L. A. Barrios, D. Aguilà, S. J. Teat, O. Roubeau, C. Bo and G. Aromí, *Chem., Eur. J.* 2017, **23**, 5117-5125.
58. D. Aguilà, V. Velasco, L. A. Barrios, J. González-Fabra, C. Bo, S. J. Teat, O. Roubeau and G. Aromí, *Inorg. Chem.* 2018, **57**, 8429-8439.
59. L. Abad Galán, D. Aguilà, Y. Guyot, V. Velasco, O. Roubeau, S. J. Teat, M. Massi and G. Aromí, *Chem., Eur. J.* 2021, **27**, 7288-7299.
60. D. Aguila, V. Velasco, L. A. Barrios, J. Gonzalez-Fabra, C. Bo, S. J. Teat, O. Roubeau and G. Aromi, *Inorg. Chem.* 2018, **57**, 8429-8439.
61. J. Gonzalez-Fabra, N. A. G. Bandeira, V. Velasco, L. A. Barrios, D. Aguila, S. J. Teat, O. Roubeau, C. Bo and G. Aromi, *Chem., Eur. J.* 2017, **23**, 5117-5125.
62. L. Abad Galán, D. Aguilà, Y. Guyot, V. Velasco, O. Roubeau, S. J. Teat, M. Massi and G. Aromí, *Chem., Eur. J.* 2021, **27**, 7288 –7299.
63. F. Luis, P. J. Alonso, O. Roubeau, V. Velasco, D. Zueco, D. Aguilà, J. I. Martínez, L. A. Barrios and G. Aromí, *Commun. Chem.* 2020, **3**, 176.
64. P. D'Angelo, A. Zitolo, V. Migliorati, G. Chillemi, M. Duvail, P. Vitorge, S. Abadie and R. Spezia, *Inorg. Chem.* 2011, **50**, 4572-4579.
65. N. Andre, R. Scopelliti, G. Hopfgartner, C. Piguet and J. C. G. Bunzli, *Chem. Commun.* 2002, 214-215.
66. S. Floquet, M. Borkovec, G. Bernardinelli, A. Pinto, L.-A. Leuthold, G. Hopfgartner, D. Imbert, J.-C. G. Bünzli and C. Piguet, *Chem., Eur. J.* 2004, **10**, 1091-1105.
67. F. Artizzu, F. Quochi, L. Marchiò, E. Sessini, M. Saba, A. Serpe, A. Mura, M. L. Mercuri, G. Bongiovanni and P. Deplano, *J. Phys. Chem. Lett.* 2013, **4**, 3062-3066.
68. F. Artizzu, F. Quochi, L. Marchiò, R. F. Correia, M. Saba, A. Serpe, A. Mura, M. L. Mercuri, G. Bongiovanni and P. Deplano, *Chem., Eur. J.* 2015, **21**, 3882-3885.
69. F. Artizzu, A. Serpe, L. Marchiò, M. Saba, A. Mura, M. L. Mercuri, G. Bongiovanni, P. Deplano and F. Quochi, *J. Mater. Chem., C* 2015, **3**, 11524-11530.
70. S. Faulkner and S. J. A. Pope, *J. Am. Chem. Soc.* 2003, **125**, 10526-10527.
71. M. S. Tremblay and D. Sames, *Chem. Commun.* 2006, 4116-4118.
72. L. S. Natrajan, A. J. L. Villaraza, A. M. Kenwright and S. Faulkner, *Chem. Commun.* 2009, 6020-6022.
73. N. Souri, P. Tian, C. Platas-Iglesias, K.-L. Wong, A. Nonat and L. J. Charbonnière, *J. Am. Chem. Soc.* 2017, **139**, 1456-1459.
74. A. Nonat, S. Bahamyirou, A. Lecointre, F. Przybilla, Y. Mély, C. Platas-Iglesias, F. Camerel, O. Jeannin and L. J. Charbonnière, *J. Am. Chem. Soc.* 2019, **141**, 1568-1576.
75. C. D. Buch, S. H. Hansen, D. Mitcov, C. M. Tram, G. S. Nichol, E. K. Brechin and S. Piligkos, *Chem. Sci.* 2021, **12**, 6983-6991.
76. M. P. Placidi, A. J. L. Villaraza, L. S. Natrajan, D. Sykes, A. M. Kenwright and S. Faulkner, *J. Am. Chem. Soc.* 2009, **131**, 9916-9917.
77. M. Suchý, A. X. Li, R. Bartha and R. H. E. Hudson, *Tetrahedron Letters* 2010, **51**, 1087-1090.
78. T. J. Sørensen, M. Tropiano, O. A. Blackburn, J. A. Tilney, A. M. Kenwright and S. Faulkner, *Chem. Commun.* 2013, **49**, 783-785.
79. T. J. Sørensen, M. Tropiano, A. M. Kenwright and S. Faulkner, *Eur. J. Inorg. Chem.* 2017, **2017**, 2165-2172.
80. V. Velasco, L. A. Barrios, M. Schütze, O. Roubeau, F. Luis, S. J. Teat, D. Aguilà and G. Aromí, *Chem., Eur. J.* 2019, **25**, 15228-15232.
81. B. M. Terhal, *Rev. Mod. Phys.* 2015, **87**, 307-346.
82. D. G. Cory, M. D. Price, W. Maas, E. Knill, R. Laflamme, W. H. Zurek, T. F. Havel and S. S. Somaroo, *Phys. Rev. Lett.* 1998, **81**, 2152-2155.
83. E. Macaluso, M. Rubín, D. Aguilà, A. Chiesa, L. A. Barrios, J. I. Martínez, P. J. Alonso, O. Roubeau, F. Luis, G. Aromí and S. Carretta, *Chem. Sci.* 2020, **11**, 10337-10343.
84. L. A. Barrios, D. Aguilà, O. Roubeau, P. Gamez, J. Ribas-Ariño, S. J. Teat and G. Aromí, *Chem., Eur. J.* 2009, **15**, 11235-11243.
85. L. A. Barrios, D. Aguilà, O. Roubeau, K. S. Murray and G. Aromí, *Aust. J. Chem.* 2009, **62**, 1130-1136.
86. M. D. Jenkins, D. Zueco, O. Roubeau, G. Aromí, J. Majer and F. Luis, *Dalton Trans.* 2016, **45**, 16682-16693.